Pulse-Width Modulation of Gene Expression in Budding Yeast

Rainer Machné[1,2,*], **Douglas B. Murray**[3,4], **Stephan H. Bernhart**[5], **Ilka M. Axmann**[1], **Peter F. Stadler**[5,6,7,8,9]

***For correspondence:**
machne@hhu.de (RM);
mabawsa@gmail.com (DBM)

[1]Institute for Synthetic Microbiology and; [2]Institute for Quantitative and Theoretical Biology, Heinrich Heine University, D-40225 Düsseldorf, Germany; [3]Lakeland University Japan, Shinjuku-ku, Tokyo 160-0022, Japan; [4]University of Maryland Global Campus—Asia, Yokota Air Base, Fussa-shi, Tokyo 197-0001, Japan; [5]Bioinformatics Group, Department of Computer Science, Interdisciplinary Center for Bioinformatics, Universität Leipzig, Härtelstraße 16-18, D-04107 Leipzig, Germany; [6]Max Planck Institute for Mathematics in the Sciences, Inselstraße 22, D-04103 Leipzig, Germany; [7]Institute for Theoretical Chemistry, University of Vienna, Währingerstraße 17, A-1090 Wien, Austria; [8]Facultad de Ciencias, Universidad Nacional de Colombia, Sede Bogotá, Colombia; [9]Santa Fe Institute, 1399 Hyde Park Road, Santa Fe NM 87501, USA

Abstract

Metabolic oscillations are characterized by alternating phases of high and low respiratory activity, associated with transcription of genes involved in biosynthetic pathways and growth, and in catabolism and stress response. However, the functional consequences of transcriptome oscillations remain unclear, since most proteins are too stable to be affected by oscillatory transcript abundances. In this work, we investigate a transcriptome time series during an unstable state of the oscillation. Our analyses confirm previous suggestions that the relative times spent in the alternative transcription states are coupled to growth rate. This pulse-width modulation of transcription provides a simple mechanism for the long-standing question of how cells adjust their ribosome content and growth rate to environmental conditions. A mathematical model of this idea reproduces both the almost linear relation of transcript and protein abundances and the non-linear relation of oscillation periods to growth rate.

Introduction

When yeast cultures are grown to a high cell density they tend to show collective metabolic dynamics, alternating between phases of high oxygen consumption (HOC) and low oxygen consumption (LOC). Numerous studies have shown that these oscillatory dynamics propagate throughout the metabolome, transcriptome and impinge on chromatin organization. The cycle period is dependent on growth conditions and the strain employed. Long period cycles (periods $\tau_{osc} = 3\,\mathrm{h}–8\,\mathrm{h}$) were explained by a partial synchronization of the cell division cycle (CDC). Glycogen stores are filled during LOC phase, which corresponds to the G1 phase of the CDC, and mobilized during HOC phase, which corresponds to the budding phase (***Küenzi and Fiechter, 1969***; ***von Meyenburg, 1969a***; ***Sonnleitner and Käppeli, 1986***; ***Münch et al., 1992***; ***Bellgardt, 1994***; ***Hjortso and Nielsen, 1995***; ***Futcher, 2006***). ***Satroutdinov et al.*** (***1992***) then observed much shorter periods in the strain IFO 0233 ($\tau_{osc} = 0.7\,\mathrm{h}–1\,\mathrm{h}$). IFO 0233, a distillery strain, questioned these prior models, as the glycogen storage cycle is reversed between the phases and ethanol is produced in LOC phase.

However, a similar temporal program is observed in both short period and long period experimental systems (***Machné and Murray, 2012***). Both show maxima of the cellular ATP/ADP ratio, followed by amino acid synthesis and a TORC1-mediated pulse of protein translation during the HOC phase (***von Meyenburg, 1969b***; ***Satroutdinov et al., 1992***; ***Hans et al., 2003***; ***Xu et al., 2004***; ***Müller, 2006***; ***Murray et al., 2007***; ***Machné and Murray, 2012***; ***Amariei et al., 2014***; ***O' Neill et al., 2020***). Global remodeling of promoter and gene body nucleosome organization occurs during the late LOC phase (***Amariei et al., 2014***; ***Nocetti and Whitehouse, 2016***). During the HOC phase, transcription progresses from a ribosome biogenesis cohort (`Ribi`) and cytoplasmic ribosomal protein genes (`RP`), to amino acid synthesis genes (`AA`) and mitochondrial ribosomal protein genes (`mtRP`) at the transition to the LOC phase. During the LOC phase, transcripts of a large group of stress-response and catabolic proteins (`S/C`) peak (***Klevecz et al., 2004***; ***Tu et al., 2005***; ***Slavov et al., 2011***; ***Machné and Murray, 2012***).

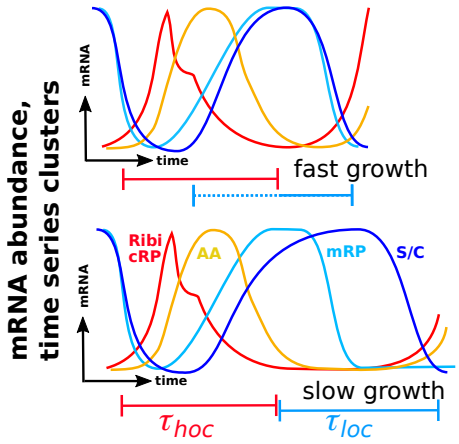

Figure 1. PWM, Pulse-Width Modulation of Transcription: The oscillation period in continuous culture is related to the culture growth rate. At slower growth the period is longer, reflected in a longer LOC phase, while the HOC phase stays approximately constant. The conserved temporal program of transcription is coupled to HOC and LOC phases. Thus, at a longer LOC phase the LOC phase-specific transcript abundances stay high for a longer time. This should lead to a overall higher abundance of LOC phase-specific transcripts (cohort `S/C`) and lower abundance of HOC phase-specific transcripts (cohort `Ribi/RP`), and thereby also to higher and lower abundances of the protein products produced (translated) from these transcripts. This is equivalent to the modulation of visually perceived intensity of LED lights by varying the fraction of time they are switched on, i.e., the pulse width.

Several hypotheses on putative functions of the temporal transcription program have been suggested. The functional profiles of co-expressed cohorts match metabolic activity, and the initial hypothesis was a "just-in-time" model of gene expression (JIT), where enzymes are expressed when required within the metabolic cycle (***Klevecz et al., 2004***; ***Tu et al., 2005***; ***Murray et al., 2007***). However, protein half-lives in yeast are now thought to be much longer than initially reported (***Christiano et al., 2014***). This dampens the effect of periodic transcript on protein abundances (***Lück et al., 2014***). Indeed, recent proteomic studies found no (**preprint:** ***Feltham et al.*** (***2019***)) or only few (***O' Neill et al., 2020***) periodic protein abundances in long period systems. ***Slavov and Botstein*** (***2011***) and ***Burnetti et al.*** (***2016***) suggested an alternative hypothesis, based on the observation that the relative duration of the LOC phase varies strongly with growth rate while HOC phase duration only subtly changes. This would result in different absolute abundances of the proteins produced from HOC- and LOC-specific transcripts and could underlie growth rate-dependent cellular resource allocation (***Maaløe, 1979***; ***Molenaar et al., 2009***). Due to the analogy to electrical engineering we refer to this idea as the pulse-width modulation (PWM) hypothesis (Fig. 1).

To test above (non-exclusive) hypotheses, we performed strand-specific RNA sequencing (RNAseq) in high temporal resolution during an unstable state of the short period cycle of the strain IFO 0233. Only a few genes that combine high transcript abundance amplitudes with short protein half-lives are compatible with the JIT hypothesis. These may point to a feedforward control of the transition from catabolic to anabolic flux. However, the bulk of the protein-coding transcriptome codes for long-lived proteins. The duration of the LOC phase transcript abundance peak increased, and the duration of the HOC phase transcript abundance peak decreased within just two cycles of the oscillation. This preceded the transition to a longer period, compatible with the PWM hypothesis. Finally, we present a novel mathematical model of the PWM hypothesis that correctly predicts the correlations of growth-related protein abundances and oscillation periods to growth rate.

Results and Discussion

Metabolic Context: Period Drift and a Bifurcation

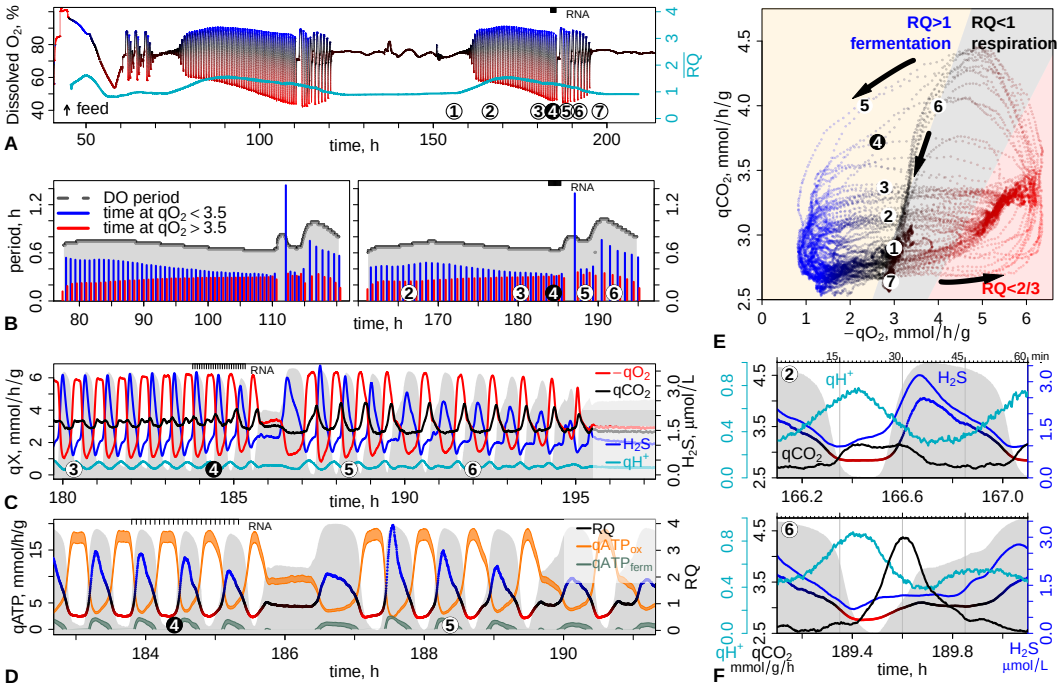

Figure 2. Complex Dynamics: Slow Transients and a Sudden Bifurcation. Metabolic dynamics during continuous culture of the budding yeast strain IFO 0233: panel A shows the full recorded time-series of the culture, and panels B–F zoom in on the time axis; bullet points P1–P7 serve as a guide between panels and are discussed in the text. The gray backgrounds show the dissolved O_2 concentration (see A for axis) and serves as a reference to oscillation phase. **A:** Dissolved O_2 (DO) measurement from the start of continuous feeding (dilution rate $\phi = 0.089\,\mathrm{h}^{-1}$). Line colors are derived from the respiratory quotient RQ (D) and indicate phases of high O_2 consumption (HOC: red) and low O_2 consumption (LOC: blue). The cyan line and right axis show the temporal mean $\overline{\mathrm{RQ}}$, a moving average over ca. 10 h. **B:** The cycle periods were derived from a Wavelet transform of the DO signal and the phase lengths are the time spans of each cycle where oxygen uptake ($-q_{O_2}$) stayed below (red, HOC) or above (blue, LOC) $3.5\,\mathrm{mmol/h/g_{DCW}}$. **C:** Zoom on P3–P6 for measured metabolic rates and concentrations; q_{O_2}, q_{CO_2} and H_2S were measured in the offgas of the reactor, corrected for the measurement delay and H_2S concentration was derived via its solubility. Proton export (q_{H^+}) was calculated from the NaOH addition rate. **D:** Zoom on P4–P5 for calculated rates. The respiratory quotient (RQ) and ATP production rates by respiration ($q_{\mathrm{ATP\,ox}}$) or by fermentation ($q_{\mathrm{ATP\,ferm}}$) were calculated from q_{O_2} and q_{CO_2} (Eq. S9–S14 in Appendix A). The RQ color gradient serves as a reference in (A, E,F). **E:** Phase portrait of q_{O_2} and q_{CO_2} over the time range indicated by bullet points in (A); points are colored by RQ (D) and in $10\,\mathrm{s}$ resolution; background colors indicate RQ ranges and arrows indicate time direction. **F:** One-hour snapshots at different times (bullet points 2 and 5). Data are indicated by colored axes and labels, except for RQ which is shown without axis but color-coded (red-black-blue) as in D and E. All reactor data is available as Datafile S1.

Previously, stable oscillations have been used to elucidate the transcriptome dynamics of continuously grown yeast (***Klevecz et al., 2004***; ***Li and Klevecz, 2006***). Here we observed more complex transient dynamics, that occurred spontaneously (Fig. 2A, S1-S3). We first calculated the oscillation periods and metabolic rates from real-time measurements of the culture (Appendix A, Dataset S1) to characterize these dynamics. The culture cycled between a phase of low oxygen consumption (LOC) and a phase of high oxygen consumption (HOC). The period was $0.6\,\mathrm{h}$–$0.7\,\mathrm{h}$ (Fig. 2B-C), i.e., the typically observed period for this strain and condition (***Satroutdinov et al., 1992***; ***Murray et al., 2001***). The respiratory quotient, $\mathrm{RQ} = \frac{q_{CO_2}}{-q_{O_2}}$, allows to infer details of the catabolic flux. During the LOC phase $RQ > 1$, i.e., cells produced ethanol and excess CO_2 (fermentation). During the HOC phase, RQ decreased below $\frac{2}{3}$, i.e., below the stoichiometry of complete ethanol oxidation (Fig. 2D). This is consistent with a re-uptake of ethanol during the HOC phase (***Satroutdinov et al., 1992***) but

points to additional contributions to CO_2 turnover, i.e., an additional uptake of CO_2 during HOC phase. Proton export (q_{H^+}, Fig. 2C, E) peaked in early HOC phase, consistent with a higher intracellular pH during HOC in both short period and long period oscillations (***Keulers et al., 1996a***; ***O' Neill et al., 2020***). The concentration of H_2S peaked at $\approx 3\,\mu M$ with a sharp increase upon transition to LOC (Fig. 2C, F), consistent with its release during amino acid biosynthesis in this transition phase (***Murray et al., 2007***) and its suggested role in population synchronization (***Murray et al., 2003***). The estimated ATP turnover rates (Fig. 2D) were in phase with previously measured ATP/ADP ratios, peaking in early to mid HOC phase (***Machné and Murray, 2012***; ***Amariei et al., 2014***). Thus, the overall properties of the oscillations were consistent with previous data. During the whole run, oscillations appeared and vanished spontaneously twice. Both these events were similar. First, period decreased from $0.7\,h$ to $0.6\,h$ within $\approx 30\,h$ (Fig. 2B). This period decrease was reflected in a decrease of the LOC phase length, while the HOC phase length even increased. At the end of this transient a sudden bifurcation of the dynamics occured. Afterwards periods were longer with a maximum of $1\,h$, but the oscillation was unstable and disappeared within a few cycles. This bifurcation was preceded by an increased and phase-shifted peak of CO_2 release at the transition from HOC to LOC (Fig. 2C, E, F). The peak of H_2S release was delayed, and a novel third phase appeared between the peaks of CO_2 and H_2S release. This intermediate phase was purely respiratory at $RQ = 1$, and all metabolic rates had intermediate values.

In summary, our experiment reflects the previously studied oscillation of the IFO 0233 strain, however, we describe complex transient dynamics that appeared twice. Emergence and disappearance of the oscillations could originate from a loss of oscillatory metabolic dynamics in single cells. We favor the alternative hypothesis that culture level oscillations result from a synchronization between individually oscillating single cells (***Silverman et al., 2010***). During the synchronous phases, the oscillation period first drifted slowly to a minimum of $\approx 0.6\,h$; then system dynamics rapidly changed (bifurcated) to an unstable state with a longer period ($\approx 1\,h$) and an intermediate phase that was purely respiratory ($RQ \approx 1$). Low but purely respiratory activity at $RQ \approx 1$ is characteristic of the LOC phase in CDC-coupled (long period) systems (***Münch et al., 1992***). The bifurcation was accompanied by the appearance of a pulse of CO_2 release before, and a delayed pulse of H_2S release after the intermediate $RQ \approx 1$ phase. We interpret the period drift and sudden transition as an imbalance between catabolic and anabolic flux.

Transcriptome Oscillation: A Universal Temporal Program

Numerous time series of the protein-coding transcriptome have revealed a universal temporal program of defined transcript cohorts but with periods ranging from $40\,min$ to $7.5\,h$ (***Machné, 2017***). Transient states of the oscillation or non-coding transcription have not been studied. We sampled for RNAseq analysis every $4\,min$ for 2.5 cycles, just preceding the bifurcation of system dynamics (P4 in Fig. 2). The strand-specific sequencing reads were mapped to the reference genome (strain S288C, R64-1-1), yielding reads for $76\,\%$ of the genome (Fig. S5A). A similarity-based segmentation algorithm (***Machné et al., 2017***) yielded ca. 37k segments (Fig. S5D), each a putative individual transcript. All segments were classified by their oscillation p-values, calculated with the `rain` package (***Thaben and Westermark, 2014***), and by their overlaps with annotated genome features (Tab. S2). 4,489 segments were classified as open reading frame (ORF) transcripts; 3,378 of these showed oscillation and reproduced the previously characterized temporal sequence (Fig. 3A; ***Machné and Murray*** (***2012***)). Oscillating non-coding (811 of 9,051) and antisense (232 of 569) segments predominantly peaked in the LOC phase. Very short and weakly expressed segments were removed from further analyses, the remaining 11k segments (Fig. S5G–I) were clustered into ten co-expressed clusters, and these were sorted and colored by their peak phase (Fig. S6–S8). These ten clusters can be further classified (Fig. S6C) into two groups of five clusters each. The first group (Fig. 3B) comprises of longer segments with high amplitudes, and most assigned to protein-coding genes (Fig. S7). The second group (Fig. 3C) contains shorter and weakly expressed segments with lower amplitudes, mostly non-coding and peaking during the LOC phase (Fig. S8).

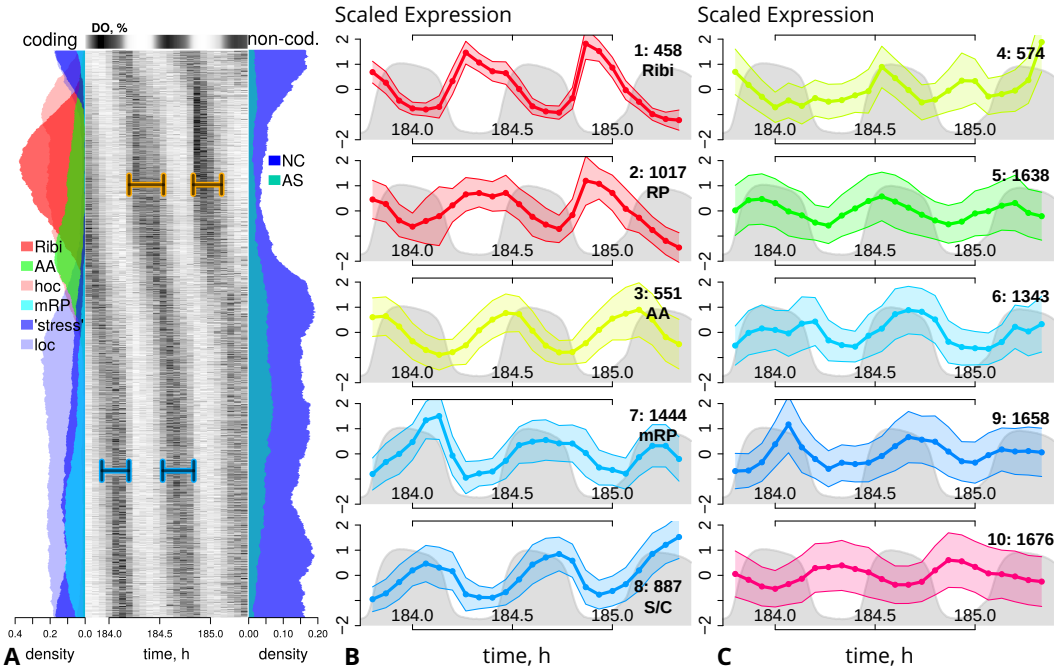

Figure 3. RNAseq Time Series Clustering. A: Phase-ordered heatmap of the time-courses of segments with oscillating abundance levels (6344 segments at $p_{\text{rain}} < 0.05$, Fig. S5E)). The dissolved O_2 (DO, %) is shown as a color gradient (black: high DO) on the top axis. Left and right panels show local densities (circular moving average of counts over 1/10 of the total number) of segments overlapping with previously defined (***Machné and Murray, 2012***) classes of coding genes (left: Ribi, ribosomal biogenesis and cytoplasmic ribosomal proteins; AA: amino acid synthesis; mRibi: mitochondrial genes, incl. ribosomal proteins; stress: catabolic and protein homeostasis genes), or non-coding segments (right: AS, antisense to ORF; NC, no overlap with any annotated transcribed feature). **B:** Time series of the five major periodic co-expression clusters. Segment time-courses (mean RPM) were scaled to a mean of 0 and divided by their standard deviation. The mean of each cluster is shown as a solid line with points indicating the sampling times, and standard deviations are shown as transparent ranges; the legends indicate the cluster label, the number of segments in the cluster and the posterior functional cohort assignment. The gray background indicates the dissolved O_2 (DO) concentration. **C:** Time series for the cluster 4, 5, 6, 9, 10, which comprise mostly non-coding segments; plotted as described for (B).

A Conserved Temporal Program Runs at Different Time Scales.

Gene Ontology (GO) enrichment analysis of the protein coding cohorts (Fig. 4A and S9) recapitulates previous data (***Klevecz et al., 2004***; ***Machné and Murray, 2012***). The ribosomal biogenesis regulon (***Jorgensen et al., 2004***) peaks in early to mid HOC phase (cluster 1: `Ribi`), followed by clusters encoding for cytoplasmic ribosomal proteins (cluster 2: `cRP`), and amino acid biosynthetic pathways (cluster 3: `AA`) at the transition to LOC phase. During the LOC phase, mitochondrial proteins, including mitochondrial ribosomal proteins (cluster 7: `mRP`) are co-expressed with a regulon associated with stress response (***Gasch et al., 2000***; ***Brauer et al., 2005***) and G1 phase (***O'Duibhir et al., 2014***). The latter comprises of proteins involved in the general stress response (chaperones) and in carbohydrate, fatty acid and protein catabolism (cluster 8: `S/C`). We used this clustering to re-analyze eight data sets from different strains and conditions and with periods ranging from 40 min to 7.5 h (Fig. S10–S11, data from ***Li and Klevecz*** (***2006***); ***Tu et al.*** (***2005***); ***Slavov et al.*** (***2011***); ***Chin et al.*** (***2012***); ***Kuang et al.*** (***2014***); ***Wang et al.*** (***2015***); ***Nocetti and Whitehouse*** (***2016***)). This meta-analysis reveals common patterns. A temporally constrained program (0.5 h–2 h) leads from `Ribi`/`cRP` *via* `AA` to `mRP`, ending with the transition from HOC to LOC phase. Increases of the total period are mostly reflected by increased duration of the LOC phase and the associated `S/C` cohort expression. The same temporal program can be observed in six distinct cell cycle arrest & release experiments (Fig. S12) (***Orlando et al., 2008***; ***Bristow et al., 2014***).

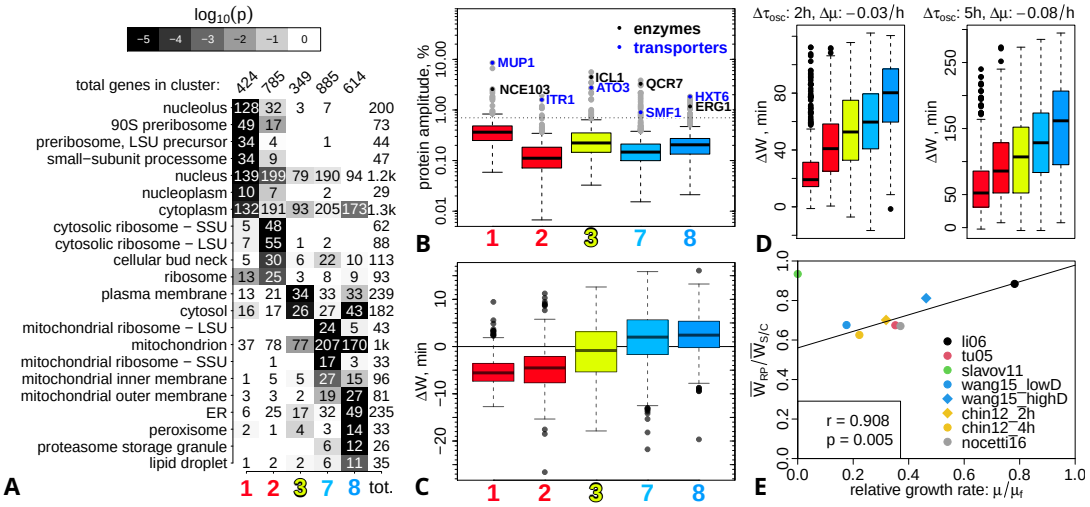

Figure 4. A Universal Temporal Program. A: Sorted cluster enrichment profiles for the GO category "cellular component". The p-values were calculated by cumulative hypergeometric distribution tests and are shown as gray-scale. Only categories with $p < 0.001$ (white text) and more then 10 genes in one of the clusters are shown. See Figure S9 for all clusters and GO categories. **B:** Boxplots of cluster distributions of predicted relative protein amplitudes (A_P, in % of their mean abundance), estimated from transcript amplitudes and protein half-lives (Fig. S13). The horizontal line indicates the the top 100 oscillators listed in Table S3. The top predicted oscillators of class enzyme or membrane transporter of each cluster are indicated. **C:** Boxplots of cluster distributions of transcript abundance peak width differences $\Delta W = W_2 - W_1$ between the second and first full expression cycle. Figure S16 provides details on the calculation. **D:** Boxplots of the transcript abundance peak width differences between two experiments from the same culture but at different growth rates (left: ***Chin et al.*** (***2012***), right: ***Wang et al.*** (***2015***)). See Fig. S10B for raw peak widths. **E:** Peak width ratio vs. growth rate for all experiments analyzed in Figure S10B. The ratio of the mean peak widths of cluster 2 ($\overline{W}_\mathrm{RP}$) and cluster 8 ($\overline{W}_\mathrm{S/C}$) is correlated to the strain-specific relative growth rate (μ/μ_f, see Fig. S10B for μ and Tab. S5 for μ_f values). Experiments are indicated by the first author and year in the legend. The line indicates a linear regression, and r and p are the Pearson correlation and p-value, all calculated without the outlier at $\mu = 0\,\mathrm{h}^{-1}$ (`slavov11`) which was taken from an oscillation at the end of a batch growth phase on ethanol medium.

Testing Hypotheses: Putative Functions of the Temporal Program

Next, we analzyed the two hypotheses on putative functions of this universal temporal program; the just-in-time production (JIT) and the pulse-width modulation (PWM) hypothesis.

Carbonic Anhydrase and the Glyoxylate Cycle are Novel Feedback Candidates.

The temporal order of mRNA abundances makes intuitive sense as a just-in-time gene expression program (JIT) coordinated with metabolic events. However, oscillations on transcript level are dampened by long protein half-lives (***Lück et al., 2014***). Thus, we estimated relative protein amplitudes (Fig. 4B, S13A–C) from our RNA abundance time series and from protein half-life data by ***Christiano et al.*** (***2014***), using a mathematical model of periodic gene expression by ***Lück et al.*** (***2014***). Most proteins are predicted to vary by 0.1 %–0.5 % of their mean abundance (Fig. 4B and S13C). Only 23 proteins have predicted relative protein amplitudes ≥2 %; and oscillators are enriched in the `Ribi` and `AA` cohorts (Fig. S13C). These low amplitudes probably do not have a strong effect on metabolic dynamics, but the model is based on sine approximations of transcript time series and protein half-lives measured in asynchronous conditions; it may understimate amplitudes and it completely neglects potential effects of induced protein degradation and post-translational modifications. Thus, we tested our predicted against measured protein amplitudes in a long period oscillation (***O' Neill et al., 2020***). The genome-wide correlation between these amplitude sets was weak but significantly positive (Fig. S14). However, the top oscillator estimates of both data sets overlapped (Fig. S13D, E). Notably, 60 of the top 100 oscillators in our analysis were not detected in the proteomics measurement. These include several transcription factors (e.g. BDF2, CLB2, GZF3,

MET28, SWI5, MSN4) which are known to be expressed at low levels. Thus, our analysis reveals putative oscillators that are potentially missed by proteomics analysis.

Both top oscillator lists share cell wall proteins, nutrient transporters, and metabolic enzymes. Several enzymes of the sulfate uptake pathway (MET genes) are expressed in `Ribi` and peaked prior to the pathway intermediate H_2S at the HOC/LOC transition (Fig. 2). The carbonic anhydrase (NCE103, in `Ribi`) catalyzes the interconversion of carbon dioxide and bicarbonate ($CO_2 + H_2O \leftrightarrow HCO_3^- + H^+$), and is essential in aerated cultures (***Aguilera et al., 2005***). During the second sampled cycle the `Ribi` cohort was downregulated early (Fig. 3A, Fig. 4C) and this correlated with the appearance of the CO_2 and the delay of H_2S release pulses at transition to LOC (Fig. 2C–F). Both, CO_2 and H_2S, were previously suggested to contribute to population synchronization (***Keulers et al., 1996a***; ***Murray et al., 1999***, ***2003***), and both are substrates of biosynthetic metabolism. However, the strongest synchronizing activity was found for the acetaldehyde (***Murray et al., 2003***), a futile intermediate of fermentation or, more generally, of overflow metabolism around the pyruvate node of metabolism, between glycolysis, respiration and biosynthesis (***Pronk et al., 1996***; ***Sonnleitner and Käppeli, 1986***). The switch from catabolism in HOC phase to anabolism at the transition to LOC phase likely involves regulation around this central node of metabolism. We find several biosynthetic enzymes among the top 100 predicted oscillators (Fig. S15), most notably three enzymes of the glyoxylate cycle (ICL1, CIT2, MDH2, all in the `AA` cohort), a shorter and purely biosynthetic version of the tricarboxylic acid cycle. It is for example required to synthesize glucose, when ethanol is the only carbon source. This cycle is autocatalytic (***Barenholz et al., 2017***) and serves as metabolic switch in response to changes in carbon source (***Nakatsukasa et al., 2015***).

All discussed pathways also appear in the proteome-based list of top oscillators (Fig. S13D,E, S14), supporting their general relevance for metabolic oscillations. As outlined in Figure S15, these short-lived enzymes could be involved in gating the transition from the catabolic to the anabolic phase of the cycle.

Resource Allocation by Pulse-Width Modulation (PWM).

Most proteins are too stable for an effect of oscillatory transcript on protein abundances. ***Slavov and Botstein*** (***2011***) and ***Burnetti et al.*** (***2016***) suggested an alternative interpretation of periodic transcription. Variation of the relative times spent in HOC phase- and LOC phase-specific transcription states could serve to tune steady-state protein abundances. The LOC phase duration decreases with increasing growth rates, while HOC phase duration remains approximately constant or even slightly increases (***von Meyenburg, 1969a***; ***Strässle et al., 1989***; ***Slavov and Botstein, 2011***; ***Burnetti et al., 2016***; ***O' Neill et al., 2020***). This would lead to a higher relative biomass fraction of proteins from HOC phase-specific transcripts, i.e. of the `Ribi` and the `cRP` cohorts. During our experiment a similar shift of the relative times spent with HOC or LOC phase-specific expression occured (horizontal bars in Fig. 3A). We quantified and compared the peak widths between the two cycles (Fig. S16). The `S/C` cohort peak width increased on average by $\approx 3\,\mathrm{min}$, while the `Ribi` cohort peak width decreased by $\approx -5\,\mathrm{min}$ (Fig. 4C). This occured without comparable changes of the duration of HOC and LOC phases, i.e., the transcription was not merely an output of respiratory dynamics. Thus, the relative duration of expression phases can be adapted rapidly and affect the metabolic dynamics in subsequent cycles.

So we next looked for evidence of PWM of transcription in the previous data sets and calculated peak widths for all transcripts (Fig. S10B). When growth rate was decreased in dilution rate shift experiments (***Chin et al., 2012***; ***Wang et al., 2015***) the period increased, as expected. Most transcript abundance peak widths increased with period, but this increase was significantly higher for the LOC-phase specific cohorts (Fig. 4D). Thus, the peak widths of HOC phase-specific and LOC phase-specific co-expression cohorts indeed changed with growth rate. The oscillation periods tend to reach a minimum towards a strain-specific critical growth rate (μ_f) where fermentation sets in (***Burnetti et al., 2016***; ***Machné et al., 2017***). We calculated the mean peak widths of the `RP` cohort (cluster 2) and the `S/C` cohort (cluster 8), and a relative growth rate for each experiment,

i.e., the growth rate (dilution rate) of the continuous culture divided by the strain-specific critical growth rate ($\frac{\mu}{\mu_f}$). This reveals a good correlation between the RP to S/C peak width ratio and the relative growth rate of the cultures (Fig. 4E). The only outlier is the transcriptome data taken at the end of a batch growth phase, i.e. at $\mu \approx 0\,\mathrm{h}^{-1}$, on ethanol medium (***Slavov et al., 2011***).

An increase of ribosome content is directly and causally related to higher growth rates, constituting a fundamental principle of microbial growth physiology (***Schaechter et al., 1958***; ***Waldron and Lacroute, 1975***; ***Koch, 1988***; ***Scott et al., 2010***). This relation is reflected in continuous changes of relative abundances of different transcript and protein classes with growth rate (***Brauer et al., 2005***; ***Airoldi et al., 2009***; ***Molenaar et al., 2009***; ***Metzl-Raz et al., 2017***). No mechanism for this continous variation of gene expression is known in eukaryotes. A temporal regulation, via continuous changes of the relative durations of LOC and HOC phases generates this relation in synchronously oscillating continous culture. Even in asynchronous cultures, individual cells appear to oscillate (***Silverman et al., 2010***), thus this mechanism is likely general.

The PWM Model Explains Period and Proteome Relations to Growth Rate

Consistent Prediction of Transcript and Protein Abundances.

Next, we set out to explore the predictive power of the PWM hypothesis. In short, we assume a step function of transcriptional activity, such that genes are transcribed at maximal rate during their respective expression phase (HOC or LOC) and not transcribed in the other phase. The mean concentrations (over time) of an mRNA that is transcribed only in HOC phase (R_{hoc}), and of its protein product (P_{hoc}) are:

$$\begin{aligned} R_{hoc} &= \frac{\phi_{hoc} k}{\mu + \delta_r} \\ P_{hoc} &= R_{hoc} \frac{n_B \ell}{\mu + \delta_p}\,, \end{aligned} \tag{1}$$

where $\phi_{hoc} = \tau_{hoc}/\tau_{osc}$ is the fraction of the total period (τ_{osc}) spent in HOC phase (τ_{hoc}), k and ℓ are transcription and translation elongation rates, n_B is the ribosome density (ribosomes per RP mRNA); δ_r and δ_p are the mRNA and protein degradation rates; and μ is the culture growth rate. The same model can be used for LOC phase-specific genes, with transcription restricted to $\phi_{loc} = 1 - \phi_{hoc}$. See Appendix B for a detailed derivation of the model.

The period τ_{osc} decreases with increasing growth rate (Fig. 5A, S17A). This period decrease is reflected in a decrease of the time spent in LOC phase (τ_{loc}), while the duration of the HOC phase stays approximately constant or even slightly increases (***von Meyenburg, 1969a***; ***Strässle et al., 1989***; ***Bellgardt, 1994***; ***Slavov and Botstein, 2011***; ***Burnetti et al., 2016***; ***O' Neill et al., 2020***). Similarly, τ_{loc} decreased with period τ_{osc}, while τ_{hoc} changed less and in opposite direction during our experiment (Fig. 2B). We thus estimated a $\phi_{hoc} = f(\mu)$ from data from the IFO 0233 strain (Fig. 5A, ***Murray et al.*** (***2001***)), used our classification into HOC phase and LOC phase genes (Fig. 3, 4), and collected gene-specific parameters for the production and degradation rates for each gene (Fig. S18). The model assumes that all regulation occurs through initiation of transcription at a maximal rate in HOC or LOC phase. The maximal transcription and translation rates merely depend on the gene and proteins lengths, while ribosome densities (per mRNA) and degradation rates are derived from genome-wide experimental data (Tab. S5). These assumptions and data allowed to estimate growth rate-dependent mean transcript and protein abundances from Eq. 1 for 1,197 genes (Fig. 5C–F, S21). To estimate the predictive power we calculated the slopes $\frac{d\mathrm{mRNA}}{d\mu}$, and find a good correlation (Spearman's $\rho = 0.66$) with the slopes reported for 35 signature genes of the Universal Growth Rate Response (UGRR) model (Fig. 5D, ***Airoldi et al.*** (***2009***); ***Slavov and Botstein*** (***2011***)). Next, we calculated slopes for absolute transcript counts measured in chemostat cultures at different growth rates by ***Xia et al.*** (***2022***). The correlation is overall weak ($\rho = 0.35$, Fig. S21C), but better for smaller gene sets from a more stringent consensus classification ($\rho = 0.74$, Fig.

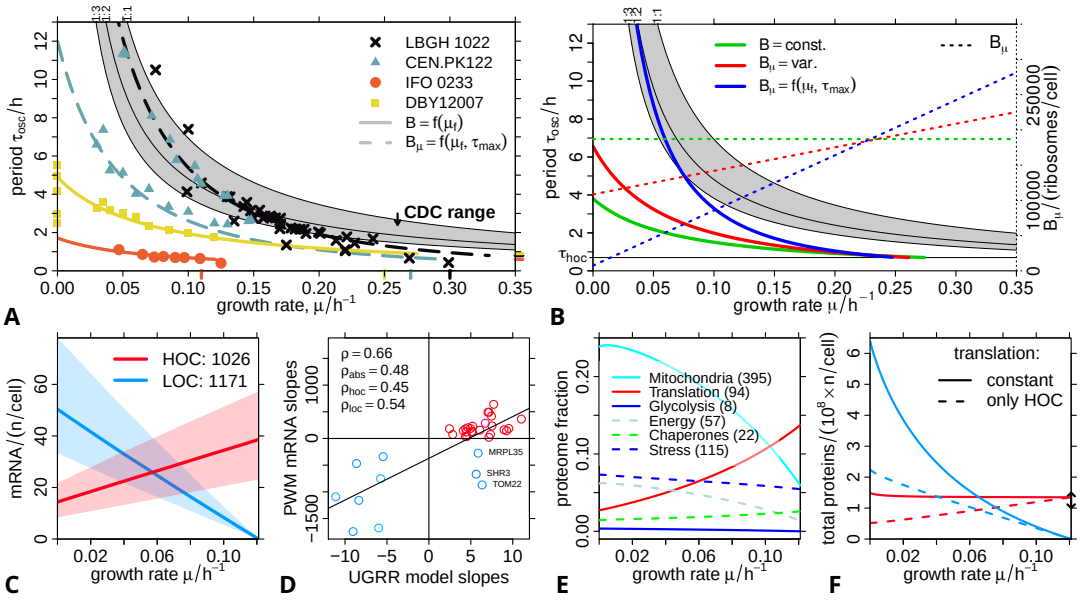

Figure 5. The PWM Model. A: Oscillation periods are non-linearly related to growth rate, here shown for four different strains (colored points, cf. Fig. S17A). The periods expected from partial CDC-synchronization (CDC range) in modes 1:1, 1:2 and 1:3 are shown as black solid lines (***Bellgardt, 1994***), via Eq. S31-S32. The PWM model (colored lines, Tab. S6) can re-produce the observed periods, incl. at $\mu \to 0$, and the relation to the strain-specific critical growth rate μ_f (colored ticks on the x-axis). Solid lines indicate a PWM model with constant ribosome concentration calculated via μ_f, and dashed lines with linearly increasing ribosome concentration and the additional assumption of a τ_{max}; τ_{hoc} (colored ticks on the right y-axis) was manually adjusted. **B:** Periods predicted by the base model (Eq. 2, solid green line) and the extended model with variable ribosome concentration $B(\mu)$ (Eq. S25, solid red line), with parameters from Table S5. The colored dashed lines are the ribosome concentrations (right y-axis) used for each model. Alternatively, ribosome parameters can be estimated via the μ_f-constraint (Eq. S26, solid blue line). **C:** Median (lines) and 25%/75% quantiles (transparent range) of all mRNA abundances predicted by the PWM model (Eq. 1) from ϕ_{hoc} (IFO 0233 parameters in (A)), and from gene-specific production and degradation rates (Tab. S18B), and classification to either HOC (clusters 1, 2 and 10) or LOC (clusters 6, 7, 8 and 8) phase. The legend indicates the number of genes for which all data was available. **D:** Comparison of the mRNA slopes, derived from a linear regression of the data in (C), and the slopes provided for signature genes of the UGRR model (***Slavov and Botstein, 2011***). All data required for the PWM-based prediction was available for the shown 35 of 58 signature genes. Gene names are provided for the outliers, two mitochondrial and one ER-associated. The straight line is a linear regression, and ρ is the Spearman correlation, ρ_{abs} removes the influence of the classification by taking the absolute slopes in both data sets, and ρ_{hoc} and ρ_{loc} are correlations calculated for only the HOC- or LOC-specific signature genes (red and blue point symbols). **E:** Fractions of the total protein abundance predicted by the PWM model (Eq. 1) for the gene lists used to analyze proteome fractions in ***Metzl-Raz et al.*** (***2017***); gene numbers in brackets. **F:** Total protein abundances predicted by the PWM model for HOC and LOC phase genes ; calculated without (solid lines, Eq. 1) or with (dashed lines, Eq. S27) an additional restriction of translation to HOC phase. The vertical black arrow indicates the total protein content estimation by ***Milo*** (***2013***). All rates required for mRNA and protein prediction are available in Dataset S3.

S21D). Similarly, we found good overall agreement of the relative proteome fractions at different growth rates of gene groups selected by ***Metzl-Raz et al.*** (***2017***) (Fig. 5E). For example, the proteome fraction of mitochondrial genes decreases, while the fraction of genes involved with translation increases with growth rate, reflecting measurements (***Metzl-Raz et al., 2017***). The correlation with measured growth rate-slopes of proteins (***Xia et al., 2022***) were higher than for transcripts ($\rho = 0.42$, and $\rho = 0.78$ for the consensus set; Fig. S21G,H). However, the strongest contribution to these correlations comes from our accurate classification into HOC and LOC phase genes, while the correlation for the HOC phase-specific transcripts was even negative (Fig. S21C).

The model neglects all other types of regulation such as targeted degradation, or intrinsic bias such as sequence-dependent differences of elongation rates; thus, it is not suprising that on a

genome-wide scale the predictive power is weak. Appendix B.6 discusses potential reasons for these discrepancies. A more fundamental problem of the model is that translation is unlimited. The total protein abundance increases strongly at $\mu \to 0$, while it is very close to estimates from experimental data (***Milo, 2013***) at high μ (Fig. 5F). As outlined in Appendix B.5, previous data point to a pulse of translational activity at the HOC-to-LOC transition. The majority of ATP synthesis occurs in HOC phase; as a simple approximation, we restricted the translation of all transcripts (HOC and LOC phase) to HOC phase (Eq. S27). This reduced the total protein abundance at $\mu \to 0$ to about twice the estimate for cells in exponential growth (***Milo, 2013***), thus into a more realistic range.

The PWM Model Predicts Oscillation Periods.

We further noted, that the model yields a strict constraint between oscillation parameters, the life cycle rates and concentration of proteins, and growth rate. Ribosomal proteins (RP) are (a) transcribed within the HOC phase clusters (***Klevecz et al., 2004***; ***Machné and Murray, 2012***) (Fig. 4A, D), and (b) their relative fraction of total biomass increases with growth rate (Fig. S18C–E, (***Waldron and Lacroute, 1975***)). Thus, we can use this constraint to predict oscillation periods from measured ribosome concentrations and life cycle parameters. Assuming that each RP is associated with one ribosome (Appendix B.2), we get:

$$\frac{\tau_{osc}}{\tau_{hoc}} = \frac{k}{\mu + \delta_r} \frac{\ell}{\mu + \delta_p} \frac{n_B}{B(\mu)} \,, \tag{2}$$

where $B(\mu)$ is the total concentration of (cytoplasmic) ribosomes, and all other parameters refer to an average RP (Tab. S5, Fig. S18A). Remarkably, the collected literature parameters already yield (i) realistic periods and (ii) the non-linear dependence of periods on growth rates (green line, Fig. 5B). Linearly varying the ribosome concentration with growth rate (Fig. S18C) makes the period function steeper (red line, Fig. 5B).

Experimentally observed periods reach a minimum towards the strain-specific growth rates μ_f, where yeast metabolism switches from purely respiratory to respiro-fermentative metabolism of glucose (***Burnetti et al., 2016***; ***Machné, 2017***). In the IFO 0233 strain, fermentation sets in early, at growth rates $\mu_f = 0.11\,\mathrm{h}^{-1}$–$0.15\,\mathrm{h}^{-1}$ (***Hansson and Häggström, 1983***; ***Satroutdinov et al., 1992***) consistent with its short period cycles. This constraint allows to estimate strain-specific values for the RP and ribosome-related parameters via published values for μ_f (Appendix B.3, Fig. 5A, S17D, Tab. S6). The model with variable ribosomes is required to fit data from the two strains with longer periods (CDC range), or, alternatively, very low degradation rates (Fig. S17C). This pattern is confirmed when fitting Eq. 2 separately to 20 independent data sets (Fig. S19, S20). Long period data sets require to set at least one of the degradation parameters (δ_r, δ_p) to 0. This may be due to a phase-locking with the CDC (gray areas in Fig. 5A, B), where the HOC phase aligns with the budding phase of the CDC and LOC phase is purely respiratory (RQ ≈ 1) and corresponds to the G1 phase of the CDC (***Münch et al., 1992***). When such phase-locking with the CDC occurs, PWM and oscillation parameters may not be directly coupled anymore.

Previously suggested models based on partial synchrony of the asymmetric cell division cycle fit long period data well (***Bellgardt, 1994***; ***Hjortso and Nielsen, 1995***; ***Duboc and von Stockar, 2000***). However, these models can not account for oscillations in batch culture and without division (***Mochan and Pye, 1973***; ***Murray, 2004***; ***Slavov et al., 2011***) and for periods that are longer than the culture doubling time (***Heinzle et al., 1983***; ***Porro et al., 1988***). ***Burnetti et al.*** (***2016***) suggested a purely empirical model for these relations. The PWM model is the first mechanistic model of the oscillation that can account for all experimentally observed periods; although only with unrealistic parameter choices for long periods. Future work based on this novel theoretical framework should explicitly account for energetic constraints on the protein synthesis capacity during the cycle, and could explore the effects of additional regulatory mechanisms or systematic differences in production and degradation rates.

Conclusion

The phenomenon of metabolic auto-synchronization in budding yeast continuous culture was instrumental for the clarification of the asymmetric CDC of budding yeast (***Küenzi and Fiechter, 1969***; ***von Meyenburg, 1969a***). The discovery of stable short period cycles in the distillery strain IFO 0233 (***Satroutdinov et al., 1992***) fortified early indications (***von Meyenburg, 1969b***; ***Mochan and Pye, 1973***) that the system is more than just synchronization of the CDC. Here, we first explored the complexity of dynamics observable in budding yeast continuous culture, a long-term transient and a sudden bifurcation. We then tested the two main hypotheses on putative functions of the periodic transcriptome (JIT and PWM).

We presented four independent lines of evidence in support of the PWM hypothesis (***Burnetti et al., 2016***; ***Slavov and Botstein, 2011***): (i) transcript abundance peak widths changed as predicted in two dilution rate shift experiments, (ii) the relative peak widths correlated very well to the relative growth rate, i.e., the growth rate divided by the strain-specific critical growth rate, (iii) the PWM model predicts measured growth rate-dependent transcript and protein abundances reasonably well, despite its simplicity, and (iv) the PWM model predicts the dependence of oscillation periods on growth rate. The coupling is consistent over periods ranging from $40\,\mathrm{min}$ to $7.5\,\mathrm{h}$. We further note that circadian biology faces a similar problem, low protein abundance amplitudes despite significant transcript abundance oscillations (***Lück et al., 2014***; ***Wang et al., 2018***; ***Krahmer et al., 2021***; ***Karlsen et al., 2021***). While the period is fixed, seasonal variation of light/dark cycle phase lengths could mediate PWM-based control of steady state protein abundances.

And finally, the prediction of periodic proteins (JIT analysis) and the metabolic dynamics during our experiment underpin previous data on H_2S and CO_2 as population synchronizers (***Keulers et al., 1996a***; ***Murray et al., 2003***, ***2007***). The accumulating evidence suggests that the involved pathways could gate the switching from catabolic to anabolic flux at the transition from HOC phase to LOC phase (Fig. S15). The metabolic mechanisms behind CDC-coupled long period oscillations were considered to lie in a cycle of glycogen build-up during LOC phase and mobilization during HOC phase, where the respiratory electron transport chain becomes limiting and overflow metabolism at the pyruvate node (ethanol, acetate or acetaldehyde accumulation and secretion) induces the switch to LOC phase and synchronizes the culture (***Küenzi and Fiechter, 1969***; ***Strässle et al., 1989***; ***Münch et al., 1992***). However, glycogen content oscillates at low amplitude and peaks in the wrong phase in IFO 0233 (***Satroutdinov et al., 1992***) and glycogen is not produced during oscillatory growth on ethanol-based medium (***Keulers et al., 1996b***). Thus, the glycogen cycle model is either wrong or not generally valid. The next big question is thus to clarify the metabolic mechanisms behind switching between the HOC and LOC phases of this cycle. What is the nature of the metabolic limitation in continuous culture, and how does it determine the relative lengths of the phases?

Supporting Information and Data

The RNA sequencing reads are available at ArrayExpress (http://www.ebi.ac.uk/arrayexpress/, ***Athar et al.*** (***2019***)) with accession number E-MTAB-11901.

Supporting Information File:

Appendices A (calculation of metabolic rates from bioreactor online measurements), B (detailed formulation of the PWM model), and all Supporting Figures.

Dataset S1:

Reactor data, including all calculated rates and RNAseq sampl timess.

Dataset S2:

All 36,928 segments reported by `segmenTier`, incl. genome coordinates, cluster labels, read-counts, oscillation values (amplitude A_2, phase ϕ_2, p-value p_{rain}), coding gene and SUT overlaps, and all time points, using the sampling IDs (2–25) indicated in the reactor data.

Dataset S3:

Data for 3,849 coding genes that overlap with a segment with $J > 0$: relative mRNA and protein amplitudes and protein half-lives for prediction of protein amplitudes (Fig. S13), and production and degradation rates as used for period, mRNA and protein abundance predictions, incl. cluster associations and classification as RP gene (Fig. S18A/B, Tab. S5).

Materials and Methods

Strain History

Kuriyama's lab first reported oscillations in continuous culture of the *Saccharomyces cerevisiae* strain IFO 0233 (***Satroutdinov et al., 1992***). The strain number is from the Japanese culture collection NBRC and is identified there as "`Distillery yeast Rasse II`", "accepted" in 1941, and as ATCC 560 in the US American culture collection. These strains can be traced back to the "Brennereihefe, Rasse II" isolated as "Hefe 128" axenic culture by Paul Lindner at the Berlin Institut für Gärungsgewerbe in 1889 from samples of a distillery in Gronowo (West Prussia, now Poland) which obtained their yeast from a dry yeast supplier in the city Thorn (now Toruń, Poland) (***Lindner, 1895***). The strain and its descendant "Rasse XII" became commercially successful distillery strains within hybrid formulations ("Rasse M"), and was at the time an intensively studied strain in basic research, *e.g.*, in the search for the nature of "bios" (***Lindner, 1919***).

Continuous Culture

Pre-Culture

Saccharomyces cerevisiae (strain IFO 0233) were maintained on yeast nitrogen base agar plates (2 % glucose, 1.5 % agar; Difco, Japan) at 4 °C, sub-cultured from frozen stock cultures (-80 °C; 1 mL; 15 % glycerol; 5×10^8 cells). Pre-cultures were inoculated into Yeast Extract Peptone Dextrose media (10 mL; 1 % yeast extract, 2 % peptone, 2 % glucose) and grown at 30 °C in an orbital incubator (200 rpm) for 24 h.

Continuous Culture Medium & Inoculation

The culture medium consisted of D-glucose ($20\,\mathrm{g\,L^{-1}}$), (NH4)2SO4 ($5\,\mathrm{g\,L^{-1}}$), KH2PO4 ($2\,\mathrm{g\,L^{-1}}$), MgSO4.7H2O ($0.5\,\mathrm{g\,L^{-1}}$), CaCl2.2H2O ($0.1\,\mathrm{g\,L^{-1}}$), FeSO4.7H2O ($20\,\mathrm{mg\,L^{-1}}$), ZnSO4.7H2O ($10\,\mathrm{mg\,L^{-1}}$), CuSO4.5H2O ($5\,\mathrm{mg\,L^{-1}}$), MnCl2.4H2O ($1\,\mathrm{mg\,L^{-1}}$), 70 % H2SO4, ($1\,\mathrm{mL\,L^{-1}}$), Difco yeast extract ($1\,\mathrm{g\,L^{-1}}$) and Sigma Antifoam A ($0.2\,\mathrm{mL\,L^{-1}}$). All chemicals were supplied by Wako Pure Chemical Industries Ltd., Japan. The medium prepared with this recipe has a pH of ca. 2.5 which allows for autoclaving of media with both sugar and ammonium without browning (caramelization) and further avoids precipitation of salts in feed medium bottles during continuous culture. A custom-built bioreactor as outlined below was filled with 0.635 L of medium and autoclaved (121 °C; 15 min). Aeration ($0.15\,\mathrm{L\,min^{-1}}$), agitation (750 rpm), and temperature (30 °C) and pH (3.4) control were switched on, until the system was equilibrated. Then, the dissolved oxygen probe was 2-point calibrated by flushing with pure nitrogen (0 %) and switching back to air (100 %). The equilibrated and fully calibrated reactor was inoculated with $\approx 1 \times 10^9$ pre-culture yeast cells. A batch phase continued for ≈40 h until the cells had reached stationary phase, indicated by a sharp decrease in respiratory activity. Then continuous culture, *i.e.*, feeding with fresh medium, was initiated (at 44.5 h in Figure 2).

Culture Control & Monitoring

Continuous culture was performed in a custom-built bioreactor. The culture vessel was a jar fermentor (Eyela, Japan) with a total volume of 2.667 L. Culture volume was measured using a balance (SB16001, Mettler Toledo, Japan), and continuous dilution with fresh medium was performed using a peristaltic pump (AC2110, ATTA, Japan) with a six roller planetary design which minimizes pulsing during rotation (about 10 rpm), and medium was pumped through 1 mm tubing (inner diameter; Masterflex, Cole Palmer, USA) and a 23 gauge steel needle. This ensured that the media was introduced in a stream of <20 µL droplets and just under a droplet per second at the operating dilution

rate. Feed medium bottle weight was monitored by a balance (PMK-16, Mettler Toledo, Japan), set up to read from unstable environments and shielded from direct breezes. The culture was agitated at $750\,\mathrm{rpm}$ and aerated at $0.150\,\mathrm{L\,min^{-1}}$ by a mass flow controller (B.E. Marubishi, Japan). Dissolved oxygen was measured using an InPro 6800 sensor and pH with an InPro 3030 (both: Mettler Toledo, Japan). Culture pH was maintained at 3.4 by the automatic addition of $2.5\,\mathrm{mol\,L^{-1}}$ NaOH, and the weight of the NaOH bottle was monitored on a balance (PM400). Local control of agitation and pH was carried out by Labo controllers (B.E. Marubishi, Japan). The reactor pressure was monitored by a manometer (DM-760, Comfix, Japan) installed on a split outlet flow stream. The culture temperature was controlled at $30\,^{\circ}\mathrm{C}$ by an external sensor connected to a circulating water bath (F25-ME, Julabo, Japan). Partial pressure of oxygen and carbon dioxide in the off-gas were measured by an Enoki-III gas analyzer (Figaro engineering, Japan). The partial pressure of hydrogen sulfide in the off-gas was measured using an electrode based gas monitor (HSC-1050HL, GASTEC, Japan). Instruments were calibrated as per manufacturer's instruction.

Reactor Data Acquisition and Calculation of Metabolic Rates

Data were acquired *via* the in-house `FERMtastic` software at $0.1\,\mathrm{Hz}$. Metabolic rates were calculated as described previously (***von Meyenburg, 1969a***; ***Heinzle, 1987***; ***Verduyn et al., 1991***; ***Marison et al., 1998***; ***Murray et al., 2007***) from the online recorded data. Details and all equations are provided in Appendix A of the supporting information. All data were processed in the script `samplingSeq_2019.R` of the `yeastSeq2016` git repository. All calculated rates are provided in Dataset S1.

RNA Sequencing & Read Mapping

Sampling, RNA Extraction & Sequencing Library Generation

Total RNA was extracted as previously described (***Sasidharan et al., 2012***) from 24 samples taken every $4\,\mathrm{min}$, covering ca. 2.5 cycles of the respiratory oscillation.

Culture samples were immediately quenched in ethanol and disrupted using acid-washed zirconia/silica beads ($0.5\,\mathrm{mm}$; Tomy Seiko Co., Ltd., Japan) with sodium acetate buffer ($250\,\mu\mathrm{L}$; sodium acetate $300\,\mathrm{mM}$, Na2-EDTA $10\,\mathrm{mM}$, pH 4.5–5.0) and one volume of TE-saturated phenol (Nacalai Tesque) equilibrated with sodium acetate buffer ($250\,\mu\mathrm{L}$).

The samples were then centrifuged ($12\,000\,\mathrm{g}$, $15\,\mathrm{min}$, $4\,^{\circ}\mathrm{C}$) and the aqueous phase transferred to fresh $1.5\,\mathrm{mL}$ microcentrifuge tubes. Back-extraction was performed by adding sodium acetate buffer ($125\,\mu\mathrm{L}$) to the bead-beat tubes, vortex ($10\,\mathrm{s}$), centrifuging ($12\,000\,\mathrm{g}$, $15\,\mathrm{min}$, $4\,^{\circ}\mathrm{C}$) and adding the aqueous phase to the first aqueous phase. 2.5 volumes ice-cold $99.5\,\%$ ethanol were added to the aqueous phase and RNA/DNA precipitated at $-20\,^{\circ}\mathrm{C}$ overnight. The samples were then centrifuged ($12\,000\,\mathrm{g}$, $30\,\mathrm{min}$, $4\,^{\circ}\mathrm{C}$), the supernatant removed by aspiration, and pellets washed 3× in $500\,\mu\mathrm{L}$ $70\,\%$ ethanol and air-dried ($10\,\mathrm{min}$, room temperature). DNA was removed (RNase-Free DNase Set; Qiagen, Japan) and RNA recovered by column purification (QIAquick PCR Purification Kit; Qiagen, Japan) in $50\,\mu\mathrm{L}$ UltraPure water, and stored at $-80\,^{\circ}\mathrm{C}$ prior to analysis. Total RNA had an RNA integrity number >7 and 260nm:230nm and 260nm:230nm ratios >2.14. All cDNA libraries were then generated and sequenced by the Beijing Genome Institute (BGI), China. Strand specific cDNA libraries were created using the "dUTP method" (***Parkhomchuk et al., 2009***; ***Levin et al., 2010***) and sequencing was carried out on an Illumina 1G sequencer.

RNAseq Read Mapping

RNAseq reads were mapped against the yeast reference genome (strain S288C, release R64-1-1) using `segemehl` (version 0.1.4) (***Hoffmann et al., 2014***) with default parameters and spliced read mapping enabled. Initially unmatched reads were mapped again using the remapping tool from the `segemehl` package and the resulting files were merged. Coverage (read-counts per nucleotide) was normalized for total library size to reads-per-million (RPM) and RPM values were stored in a bedgraph file for further analysis.

RNAseq Time Series Analysis

Analysis Strategy and R Code

All analyses were performed with bash and R. The full analysis pipeline is available in a git repository at https://gitlab.com/raim/yeastSeq2016. Analysis and plotting tools developed for this work are available in an git repository with scripts and an R package available at https://github.com/raim/segmenTools. RNAseq segmentation was performed with the `segmenTier` R package (***Machné et al., 2017***), available at https://cran.r-project.org/package=segmenTier. Scripts for genome-wide data collections and mapping to the yeast S288C reference genome (release R64-1-1) as well as the `genomeBrowser` plots are available at the git repository https://gitlab.com/raim/genomeBrowser. The collection of oscillation period data and the scripts for the PWM model analysis are available at the https://gitlab.com/raim/ChemostatData repository, generated originally for ***Machné*** (***2017***).

Additional Data Sources

Genome annotations including Gene Ontology (GO) terms were taken directly from the gff genome file from the *Saccharomyces* genome database (SGD, release R64-1-1, 2011-02-08, same as for RNAseq mapping). Published transcript data sets (XUT, SUT, etc.) were also obtained from SGD for the same genome release. Protein complex annotation CYC2008 (***Pu et al., 2009***) was downloaded from http://wodaklab.org/cyc2008/resources/CYC2008_complex.tab on 2019-06-04. All other data were obtained from the supporting material of publications: half-live data for mRNAs and proteins from ***Geisberg et al.*** (***2014***) and ***Christiano et al.*** (***2014***); ribosome density data from ***Arava et al.*** (***2003***); the consensus clustering of periodically expressed transcripts from ***Machné and Murray*** (***2012***); UGRR expression data and slopes from ***Slavov and Botstein*** (***2011***); protein abundance data from ***Paulo et al.*** (***2016***), where growth rate data was sent in personal communication; and functional gene groups from (***Metzl-Raz et al., 2017***).

Discrete Fourier Transform.

A time series of N measurements $x = \{x_0, \dots, x_{N-1}\}$, taken at equally spaced time points $\{t_0, \dots, t_{N-1}\}$, can be transformed to frequency-space by the Discrete Fourier Transform (DFT):

$$X_k = \sum_{n=0}^{N-1} x_n e^{-2\pi i \frac{kn}{N}} \quad , \quad k = \{0, \dots, N-1\} \tag{3}$$

where X_k is a vector of complex numbers representing the decomposition of the original time series into a constant (mean) component (at $k = 0$) and a series of harmonic oscillations around this mean with periods P_k, amplitudes A_k and phase angles ϕ_k:

$$\begin{aligned} P_k &= (t_{N-1} - t_0)/k\,, \\ A_k &= |X_k|/N\,, \\ \phi_k &= -\text{atan2}(\text{Im}(X_k), \text{Re}(X_k))\,. \end{aligned} \tag{4}$$

All DFT were performed with R's `fft` function.

For DFT-based clustering and segmentation analysis, it proved useful to scale DFT components by the mean amplitude of all other components $k > 0$:

$$X'_{k>0} = \frac{X_{k>0}}{\overline{|X|}_{k\neq\{0,k\}}}\,, \tag{5}$$

and the constant component ($k = 0$) by the `arcsinh` transformation:

$$X'_0 = \ln\left(|X_0| + \sqrt{X_0^2 + 1}\right). \tag{6}$$

For analysis of read-count data x_n were the raw read-counts, for analysis of segments x_n were the mean of all read-counts of the segment.

The index k corresponds to the number of full cycles with period P_k in the time series. Only the first 19 time points, covering two full cycles of the oscillation were used for the calculation of phases and p-values, such that $k = 2$ reflects the main oscillation. For all plots, phases were shifted such that $\phi_2 = 0$ corresponds to the transition from LOC to HOC.

Oscillation p-Values

For calculation of oscillation p-values p_{DFT} on read-count level the time series were permutated $N_p = 10,000$ times, and random amplitude $\tilde{A}_2$ calculated. The p-value was estimated as the fraction of permutations for which the random amplitude was larger than the observed amplitude A_2 (eqn. 4). This analysis was performed with the script `genomeOscillation.R` from the `segmenTools` git repository. Oscillation p-values p_{rain} on segment level were calculated with the R package `rain` (***Thaben and Westermark, 2014***) using period $P = 0.65\,\text{h}$ and time step $\delta t = 4\,\text{min}$. This analysis was done with the script `segmentDynamics.R` from the `segmenTools` git repository.

Segmentation of RNAseq Read-Counts & Segment Classification

The data were pre-segmented into expressed and weakly expressed chromosomal domains by a previously described heuristic (***Machné et al., 2017***) with a minor correction that splits pre-segments at chromosome ends. Pre-segmentation was done with the script `presegment.R` from the `segmenTools` script collection; Figure S4 provides pre-segment length distributions and run parameters. Pre-segments were then individually split into non-overlapping segments with coherent temporal expression profiles by the `segmenTier` algorithm, using optimized parameters from our previous study (***Machné et al., 2017***). Shortly, the `arcsinh`-transformed read-count data was Fourier-transformed (Eq. 3); the first component ($k = 0$), reflecting the mean expression level, was `arcsinh`-transformed (Eq. 6); and all other ($k > 0$) components were amplitude-scaled (Eq. 5). The real and imaginary parts of the scaled DFT components $X'_{k=0,..,6}$ were then clustered into 12 groups with R's implementation of `k-means` (using the `Hartigan-Wong` method or if that failed, the `MacQueen` method). This clustering then provided the anchors for the similarity-based segmentation by the `segmenTier`, where we used the `icor` scoring function with exponent $\epsilon = 2$, length penalty $M = 150$, nuissance cluster penalty $M_0 = 100$, and nuissance cluster exponent $\nu = 3$. This combination of parameters is achieved by arguments `-trafo "ash" -dc.trafo "ash" -dft.range 1,2,3,4,5,6,7 -K 12 -Mn 100 -scores "icor" -scales 2 -M 150 -nui.cr 3` to the `runSegmentier.R` script in the `segmenTools/scripts` collection. All segments are provided in Dataset S2.

The resulting segments were then filtered and classified by their oscillation p-values (p_{rain}, see above) and their overlaps with transcribed features annotated in the reference genome (release R64-1-1), using `segmentOverlaps.R` and `segmentAnnotation.R` in the `segmenTools/scripts` collection. Overlaps were quantified as the Jaccard index, $J = \frac{I}{U}$, where I is the intersect, the number of overlapping nucleotides, and U the union, the number of nucleotides covered by both, the segment and the annotated feature. Table S2 provides details on filtering and the resulting sizes (numbers) of analyzed segment sets. Figure S5 provides the full data structure which guided these threshold choices.

Segment Clustering

The means of read-counts covered by a segment were taken as segment time series. Periodic expression was analyzed by permutation analysis and DFT and by the R package `rain`. 11,248 segments with $p_{\text{rain}} < 0.85$ were chosen for further analysis (Fig. S5E-F). The DFT of the segment time series was amplitude-scaled (Eq. 5, Fig. S6A) and the first (constant) component ($k = 0$) was `arcsinh`-transformed (Eq. 6). Real and imaginary parts of the scaled DFT components $X'_{k=0,..,6}$ were then clustered with the `flowClust` algorithm (***Lo et al., 2009***) for cluster numbers $K = 2, \ldots, 16$. The clustering with the maximal Bayesian Information Criterion, as reported by `flowClust` (Fig. S6B), was selected for further analysis. Clustering was performed by `clusterTimeseries2` function of `segmenTools` *via* the `segmentDynamics.R` script). The resulting clustering was sorted, re-labeled and colored automatically based on the means of their segments' expression phases (Eq. 4). The

clustering was further sub-divided into high-amplitude clusters enriched for coding genes and low-amplitude clusters (compare Fig. S7 and S8).

Relative Protein Amplitudes

3,189 segments overlapping with a coding region with Jaccard index $J > 0.5$ and with protein half-live ($\tau_{1/2}$) annotation in (***Christiano et al., 2014***) were considered. Proteins with half-life annotation ">=100" were treated as $\tau_{1/2} = \infty$. The relative mRNA amplitudes were calculated from the DFT X_k (Eq. 3-4) of the first 19 time points (2 full cycles) of the RNAseq read count time series as $A_\mathrm{R} = X_2/X_0$, *i.e.*, the ratio of the amplitudes of the 2^{nd} component X_2 (2 cycles) over the 0^{th} component X_0 (corresponds to the mean over all time points) of the DFT. Relative protein amplitudes A_P were then calculated with the analytical solution to an ordinary differential equation of rhythmic production, after equation S8 of (***Lück et al., 2014***), as

$$A_\mathrm{P} = A_\mathrm{R} \frac{\gamma}{\sqrt{\gamma^2 + \omega^2}}, \tag{7}$$

with angular frequency $\omega = \frac{2\pi}{\tau_{osc}}$ and $\tau_{osc} = 0.67\,\mathrm{h}$; the total protein degradation rate $\gamma = \delta_p + \mu$, where the actual protein degradation rates δ_p were taken from (***Christiano et al., 2014***); and the growth rate equals the chemostat dilution rate $\mu = \phi = 0.089\,\mathrm{h}^{-1}$. In this model, the relative amplitude A_R is assumed to directly reflect periodic production,*i.e.*, translational activity. Total amounts or translation rates are not required, and only a relative amplitude of protein amount can be calculated. Predicted protein amplitudes are provided in Dataset S3.

Transcript Abundance Peak Width Analysis

For each high-amplitude segment (2,505 segments with $p_\mathrm{rain} < 0.0001$) the time series was interpolated to 1° resolution (0.105 min), and the oscillation phase ϕ_2 (Eq. 4) was used as anchors to scan for times spent above the temporal median $\tilde{x}$ during the first and the second full cycle in the data set (horizontal arrows in Fig. 3A). These times were recorded as the peak widths W_1 and W_2. The peak width change is the difference $\Delta W = W_2 - W_1$. Only segments with peak phases with ≥60° distance to the start or end of the timeseries and where the median expression was traversed twice within one cycle were considered, resulting in 2,357 segments with ΔW values. See Figure S16 for an example and all data. Peak widths of other transcriptome data sets (Fig. S10B) were calculated for the first full cycle of each experiment, simply as the time spent above the mean of transcript abundance over the first cycle. Data that were not sampled equispaced were interpolated at equispaced time points using the minimal time step of the original sampling.

Cluster Enrichment Analyses

Cluster-Cluster Enrichment Tests

Categorical enrichments, *e.g.* coding gene co-expression cohorts *vs.* gene annotations, were analyzed by cumulative hypergeometric distribution tests (R's `phyper`) using `segmenTools`'s `clusterCluster` function and the `clusterAnnotation` wrapper for GO and and protein complex analysis, which compares overlaps of each pair of two distinct classifications into multiple classes, and stores overlap counts and p-values ("enrichment tables") for informative plots (see "Enrichment Profiles").

In these tests, the complete set of ORF annotated in the reference genome was analyzed (urn size: 5,795). Of these, 4,489 ORF that overlapped with an segment (Tab. S2) with a Jaccard index $J > 0.5$ were assigned to this segment's cluster, where non-clustered segments ($p_\mathrm{rain} \geq 0.85$) were assigned to cluster "0", and all non-overlapping ORF ($J_\mathrm{ORF,max} < 0.5$) assigned to the "n.a" cluster. For the analysis of protein complex analysis, all 5,524 ORF that overlapped with a segment with $J_\mathrm{ORF} > 0$, and the one with the maximal J_ORF was used for cluster assignment. This relaxed assignment was used to comprehensively capture complex co-expression and differential expression.

Enrichment Profiles

The results of multi-class enrichment tests (segment overlaps or cluster-cluster categorical overlaps) were visualized as colored table plots, *e.g.* Figure 4A), using `segmenTools`' function `plotOverlaps`. The total counts of overlapping pairs are plotted as text, where the text color is selected based on a p-value cutoff p_{txt} (as indicated). The background color gray level of each field scales with $\log_2(p)$, such that fields with a minimal p-value p_{min} (as indicated) are black.

For intuitively informative plots the enrichment tables were sorted. Table rows were sorted along the other dimension (table columns) such that all categories enriched above a certain threshold p_{sort} in the first column cluster are moved to the top, and, within, sorted by increasing p-values. Next, the same sorting is applied to all remaining row clusters for the second column cluster, and so on until the last column cluster. Remaining row clusters are either plotted unsorted below a red line or removed. This is especially useful to visualize enrichment of functional categories along the temporal program of co-expression cohorts, *e.g.*, Figure 4A and D. This sorting is implemented in `segmenTools`' function `sortOverlaps`.

Author Contributions

DBM designed and performed the experiment, SHB performed the RNAseq read mapping, RM and PFS developed the segmentation algorithm. RM and IMA analyzed the time series data. All authors contributed to data interpretation and to writing of the manuscript.

Acknowledgments

We thank Sarah Lück, Oliver Ebenhöh, Wolfram Liebermeister, Oliver Bodeit, Ovidiu Popa, Chilperic Armel Foko Kuate and St. Elmo Wilken for inspiring discussions of the data and critical review of the manuscript. We are grateful to Martin Senz from the Berliner Institut f. Gärungsgewerbe und Biotechnologie, a successor of Paul Lindner, for help with clarifying the origin of the IFO 0233 strain.

Funding

DBM was funded by a partnering award from Japan Science and Technology Agency, Yamagata prefectural government and the City of Tsuruoka. RM was funded by the *Deutsche Forschungsgemeinschaft*, grants AX 84/4-1 and STA 850/30-1. IMA and RM were funded by EXC-2048/1–project ID 390686111 (CEPLAS).

References

Aguilera J, Van Dijken JP, De Winde JH, Pronk JT. Carbonic anhydrase (Nce103p): an essential biosynthetic enzyme for growth of *Saccharomyces cerevisiae* at atmospheric carbon dioxide pressure. Biochem J. 2005 Oct; 391(Pt 2):311–316.

Airoldi EM, Huttenhower C, Gresham D, Lu C, Caudy AA, Dunham MJ, Broach JR, Botstein D, Troyanskaya OG. Predicting cellular growth from gene expression signatures. PLoS Comput Biol. 2009 Jan; 5(1):e1000257. doi: 10.1371/journal.pcbi.1000257.

Amariei C, Machné R, Stolc V, Soga T, Tomita M, Murray DB. Time resolved DNA occupancy dynamics during the respiratory oscillation uncover a global reset point in the yeast growth program. Microb Cell. 2014 Sep; 1(9):279–288. doi: 10.15698/mic2014.09.166.

Arava Y, Wang Y, Storey JD, Liu CL, Brown PO, Herschlag D. Genome-wide analysis of mRNA translation profiles in Saccharomyces cerevisiae. Proceedings of the National Academy of Sciences. 2003; 100(7):3889–3894. https://www.pnas.org/content/100/7/3889, doi: 10.1073/pnas.0635171100.

Athar A, Fullgrabe A, George N, Iqbal H, Huerta L, Ali A, Snow C, Fonseca NA, Petryszak R, Papatheodorou I, Sarkans U, Brazma A. ArrayExpress update - from bulk to single-cell expression data. Nucleic Acids Res. 2019 Jan; 47(D1):D711–D715. doi: 10.1093/nar/gky964.

Barenholz U, Davidi D, Reznik E, Bar-On Y, Antonovsky N, Noor E, Milo R. Design principles of autocatalytic cycles constrain enzyme kinetics and force low substrate saturation at flux branch points. Elife. 2017 Feb; 6. doi: 10.7554/eLife.20667.

646 **Bellgardt KH**. Analysis of synchronous growth of baker's yeast. Part I: Development of a theoretical model for
647 sustained oscillations. Journal of Biotechnology. 1994; 35(1):19 – 33. doi: 10.1016/0168-1656(94)90187-2.

648 **Brauer MJ**, Saldanha AJ, Dolinski K, Botstein D. Homeostatic adjustment and metabolic remodeling in glucose-
649 limited yeast cultures. Mol Biol Cell. 2005 May; 16(5):2503–2517. doi: 10.1091/mbc.E04-11-0968.

650 **Bristow SL**, Leman AR, Simmons Kovacs LA, Deckard A, Harer J, Haase SB. Checkpoints couple transcription
651 network oscillator dynamics to cell-cycle progression. Genome Biol. 2014; 15(9):446. doi: 10.1186/s13059-
652 014-0446-7.

653 **Burnetti AJ**, Aydin M, Buchler NE. Cell cycle Start is coupled to entry into the yeast metabolic cycle across
654 diverse strains and growth rates. Mol Biol Cell. 2016 Jan; 27(1):64–74. doi: 10.1091/mbc.E15-07-0454.

655 **Chin SL**, Marcus IM, Klevecz RR, Li CM. Dynamics of oscillatory phenotypes in *Saccharomyces cerevisiae* reveal a
656 network of genome-wide transcriptional oscillators. FEBS J. 2012 Mar; 279(6):1119–1130. doi: 10.1111/j.1742-
657 4658.2012.08508.x.

658 **Christiano R**, Nagaraj N, Frohlich F, Walther TC. Global proteome turnover analyses of the Yeasts *S. cerevisiae*
659 and *S. pombe*. Cell Rep. 2014 Dec; 9(5):1959–1965. doi: 10.1016/j.celrep.2014.10.065.

660 **Duboc P**, von Stockar U. Modeling of oscillating cultivations of *Saccharomyces cerevisiae*: Identification of pop-
661 ulation structure and expansion kinetics based on on-line measurements. Chemical Engineering Science.
662 2000; 55(1):149–160. doi: 10.1016/S0009-2509(99)00301-2.

663 **Feltham J**, Xi S, Murray S, Wouters M, Urdiain-Arraiza J, George C, Townley A, Roberts E, Fisher R, Liberatori S,
664 Mohammed S, Kessler B, Mellor J. Transcriptional changes are regulated by metabolic pathway dynamics
665 but decoupled from protein levels. bioRxiv. 2019; doi: 10.1101/833921.

666 **Futcher B**. Metabolic cycle, cell cycle, and the finishing kick to Start. Genome Biol. 2006; 7(4):107. doi:
667 10.1186/gb-2006-7-4-107.

668 **Gasch AP**, Spellman PT, Kao CM, Carmel-Harel O, Eisen MB, Storz G, Botstein D, Brown PO. Genomic expression
669 programs in the response of yeast cells to environmental changes. Mol Biol Cell. 2000 Dec; 11(12):4241–4257.

670 **Geisberg JV**, Moqtaderi Z, Fan X, Ozsolak F, Struhl K. Global analysis of mRNA isoform half-lives reveals stabi-
671 lizing and destabilizing elements in yeast. Cell. 2014 Feb; 156(4):812–824.

672 **Hans MA**, Heinzle E, Wittmann C. Free intracellular amino acid pools during autonomous oscillations in *Sac-*
673 *charomyces cerevisiae*. Biotechnol Bioeng. 2003 Apr; 82(2):143–151. doi: 10.1002/bit.10553.

674 **Hansson L**, Häggström MH. Effects of growth conditions on superoxide dismutase and catalase activities in
675 *Saccharomyces cerevisiae* var. ellipsoideus. Current Microbiology. 1983; 9(1):19–23. http://dx.doi.org/10.1007/
676 BF01567128, doi: 10.1007/BF01567128.

677 **Heinzle E**. Mass spectrometry for on-line monitoring of biotechnological processes. In: *Biotechnology Methods*
678 Springer; 1987.p. 1–45.

679 **Heinzle E**, Dunn IJ, Furukawa K, Tanner RD. Modelling of sustained oscillations observed in continuous culture
680 of *Saccharomyces cerevisiae*. In: Halme A, editor. *Modelling and control of biotechnical processes* International
681 Federation of Automatic Control, Helsinki, Finland: Pergamon Press; 1983. p. 57–65.

682 **Hjortso MA**, Nielsen J. Population balance models of autonomous microbial oscillations. J Biotechnol. 1995
683 Oct; 42(3):255–269.

684 **Hoffmann S**, Otto C, Doose G, Tanzer A, Langenberger D, Christ S, Kunz M, Holdt LM, Teupser D, Hackermüller
685 J, Stadler PF. A multi-split mapping algorithm for circular RNA, splicing, trans-splicing and fusion detection.
686 Genome Biol. 2014; 15(2):R34. doi: 10.1186/gb-2014-15-2-r34.

687 **Jorgensen P**, Rupes I, Sharom JR, Schneper L, Broach JR, Tyers M. A dynamic transcriptional network commu-
688 nicates growth potential to ribosome synthesis and critical cell size. Genes Dev. 2004 Oct; 18(20):2491–2505.
689 doi: 10.1101/gad.1228804.

690 **Karlsen J**, Asplund-Samuelsson J, Jahn M, Vitay D, Hudson EP. Slow Protein Turnover Explains Limited Protein-
691 Level Response to Diurnal Transcriptional Oscillations in Cyanobacteria. Frontiers in Microbiology. 2021;
692 12:820. https://www.frontiersin.org/article/10.3389/fmicb.2021.657379, doi: 10.3389/fmicb.2021.657379.

693 **Keulers M**, Satroutdinov AD, Suzuki T, Kuriyama H. Synchronization affector of autonomous short-period-
694 sustained oscillation of *Saccharomyces cerevisiae*. Yeast. 1996 Jun; 12(7):673–682. doi: 10.1002/(SICI)1097-
695 0061(19960615)12:7<673::AID-YEA958>3.0.CO;2-C.

696 **Keulers M**, Suzuki T, Satroutdinov AD, Kuriyama H. Autonomous metabolic oscillation in continuous culture of
697 *Saccharomyces cerevisiae* grown on ethanol. FEMS Microbiol Lett. 1996 Sep; 142(2-3):253–258.

698 **Klevecz RR**, Bolen J, Forrest G, Murray DB. A genomewide oscillation in transcription gates DNA replication and
699 cell cycle. Proc Natl Acad Sci U S A. 2004 Feb 3; 101(5):1200–5. doi: 10.1073/pnas.0306490101.

700 **Koch AL**. Why can't a cell grow infinitely fast? Can J Microbiol. 1988 Apr; 34(4):421–426.

701 **Krahmer J**, Hindle M, Perby LK, Mogensen HK, Nielsen TH, Halliday KJ, VanOoijen G, LeBihan T, Millar AJ. The
702 circadian clock gene circuit controls protein and phosphoprotein rhythms in Arabidopsis thaliana. Molecular
703 & Cellular Proteomics. 2021 Nov; .

704 **Kuang Z**, Cai L, Zhang X, Ji H, Tu BP, Boeke JD. High-temporal-resolution view of transcription and chromatin
705 states across distinct metabolic states in budding yeast. Nat Struct Mol Biol. 2014 Oct; 21(10):854–863. doi:
706 10.1038/nsmb.2881.

707 **Küenzi MT**, Fiechter A. Changes in carbohydrate composition and trehalase-activity during the budding cy-
708 cle of *Saccharomyces cerevisiae*. Archives of Microbiology. 1969; 64(4):396–407. doi: 10.1007/BF00417021,
709 10.1007/BF00417021.

710 **Levin JZ**, Yassour M, Adiconis X, Nusbaum C, Thompson DA, Friedman N, Gnirke A, Regev A. Comprehensive
711 comparative analysis of strand-specific RNA sequencing methods. Nat Methods. 2010 Sep; 7(9):709–715. doi:
712 10.1038/nmeth.1491.

713 **Li CM**, Klevecz RR. A rapid genome-scale response of the transcriptional oscillator to perturbation reveals a
714 period-doubling path to phenotypic change. Proc Natl Acad Sci U S A. 2006 Oct 31; 103(44):16254–9.

715 **Lindner P**. Mikroskopische Betriebskontrolle in den Gärungsgewerben: mit einer Einführung in die Hefen-
716 reinkultur, Infektionslehre und Hefenkunde, für Studierende und Praktiker bearbeitet. P. Parey; 1895.
717 https://books.google.de/books?id=1VFIAAAAYAAJ.

718 **Lindner P**. Das Biosproblem in der Hefeforschung. Berichte der Deutschen Botanischen Gesellschaft. 1919;
719 37(11):34–40. doi: 10.1111/j.1438-8677.1919.tb07801.x.

720 **Lo K**, Hahne F, Brinkman RR, Gottardo R. flowClust: a Bioconductor package for automated gating of flow
721 cytometry data. BMC Bioinformatics. 2009; 10:145. doi: 10.1186/1471-2105-10-145.

722 **Lück S**, Thurley K, Thaben PF, Westermark PO. Rhythmic degradation explains and unifies circadian transcrip-
723 tome and proteome data. Cell Rep. 2014 Oct; 9(2):741–751.

724 **Maaløe O**. Regulation of the Protein-Synthesizing Machinery—Ribosomes, tRNA, Factors, and So On. In: Gold-
725 berger RF, editor. *Biological Regulation and Development: Gene Expression* Boston, MA: Springer US; 1979.p.
726 487–542. doi: 10.1007/978-1-4684-3417-0_12.

727 **Machné R**. Temporal Organization of Growth in *Saccharomyces cerevisiae*. PhD thesis, Theoretical Biochemistry
728 Group, University of Vienna; 2017.

729 **Machné R**, Murray DB. The yin and yang of yeast transcription: elements of a global feedback system between
730 metabolism and chromatin. PLoS One. 2012; 7(6):e37906. doi: 10.1371/journal.pone.0037906.

731 **Machné R**, Murray DB, Stadler PF. Similarity-Based Segmentation of Multi-Dimensional Signals. Sci Rep. 2017
732 Sep; 7(1):12355. doi: 10.1038/s41598-017-12401-8.

733 **Marison I**, Liu JS, Ampuero S, Von Stockar U, Schenker B. Biological reaction calorimetry: development of high
734 sensitivity bio-calorimeters. Thermochimica Acta. 1998; 309(1-2):157–173.

735 **Metzl-Raz E**, Kafri M, Yaakov G, Soifer I, Gurvich Y, Barkai N. Principles of cellular resource allocation revealed
736 by condition-dependent proteome profiling. Elife. 2017 Aug; 6. doi: 10.7554/eLife.28034.

737 **von Meyenburg HK**. Energetics of the budding cycle of *Saccharomyces cerevisiae* during glucose limited aerobic
738 growth. Archives of Microbiology. 1969; 66:289–303. doi: 10.1007/BF00414585, 10.1007/BF00414585.

739 **von Meyenburg K**. Katabolit-Repression und der Sprossungszyklus von *Saccharomyces cerevisiae*. PhD thesis,
740 ETH Zürich; 1969.

741 **Milo R**. What is the total number of protein molecules per cell volume? A call to rethink some published
742 values. BioEssays. 2013; 35(12):1050–1055. https://onlinelibrary.wiley.com/doi/abs/10.1002/bies.201300066,
743 doi: https://doi.org/10.1002/bies.201300066.

744 **Mochan E**, Pye EK. Respiratory oscillations in adapting yeast cultures. Nat New Biol. 1973 Apr; 242(119):177–
745 179.

746 **Molenaar D**, van Berlo R, de Ridder D, Teusink B. Shifts in growth strategies reflect tradeoffs in cellular eco-
747 nomics. Mol Syst Biol. 2009; 5:323. doi: 10.1038/msb.2009.82.

748 **Müller D**. Model-Assisted Analysis of Cyclic AMP Signal Transduction in *Saccharomyces cerevisiae* — cAMP as
749 Dynamic Coordinator of Energy Metabolism and Cell Cycle Progression. PhD thesis, Universität Stuttgart;
750 2006.

751 **Münch T**, Sonnleitner B, Fiechter A. The decisive role of the *Saccharomyces cerevisiae* cell cycle behaviour for
752 dynamic growth characterization. J Biotechnol. 1992 Feb; 22(3):329–351.

753 **Murray DB**. On the Temporal Self-Organisation of *Saccharomyces cerevisae*. Current Genomics. 2004;
754 5(8):665–671. http://www.ingentaconnect.com/content/ben/cg/2004/00000005/00000008/art00006, doi:
755 doi:10.2174/1389202043348580.

756 **Murray DB**, Beckmann M, Kitano H. Regulation of yeast oscillatory dynamics. Proc Natl Acad Sci U S A. 2007
757 Feb; 104(7):2241–2246. doi: 10.1073/pnas.0606677104.

758 **Murray DB**, Engelen F, Lloyd D, Kuriyama H. Involvement of glutathione in the regulation of respiratory oscilla-
759 tion during a continuous culture of *Saccharomyces cerevisiae*. Microbiology. 1999 Oct; 145 (Pt 10):2739–45.

760 **Murray DB**, Klevecz RR, Lloyd D. Generation and maintenance of synchrony in *Saccharomyces cerevisiae* con-
761 tinuous culture. Exp Cell Res. 2003 Jul 1; 287(1):10–5.

762 **Murray DB**, Roller S, Kuriyama H, Lloyd D. Clock control of ultradian respiratory oscillation found during yeast
763 continuous culture. J Bacteriol. 2001 Dec; 183(24):7253–7259. doi: 10.1128/JB.183.24.7253-7259.2001.

764 **Nakatsukasa K**, Nishimura T, Byrne SD, Okamoto M, Takahashi-Nakaguchi A, Chibana H, Okumura F, Kamura
765 T. The Ubiquitin Ligase SCF(Ucc1) Acts as a Metabolic Switch for the Glyoxylate Cycle. Mol Cell. 2015 Jul;
766 59(1):22–34. doi: 10.1016/j.molcel.2015.04.013.

767 **Nocetti N**, Whitehouse I. Nucleosome repositioning underlies dynamic gene expression. Genes Dev. 2016
768 Mar; 30(6):660–672. doi: 10.1101/gad.274910.115.

769 **O' Neill JS**, Hoyle NP, Robertson JB, Edgar RS, Beale AD, Peak-Chew SY, Day J, Costa ASH, Frezza C, Causton HC.
770 Eukaryotic cell biology is temporally coordinated to support the energetic demands of protein homeostasis.
771 Nat Commun. 2020 Sep; 11(1):4706. doi: 10.1038/s41467-020-18330-x.

772 **O'Duibhir E**, Lijnzaad P, Benschop JJ, Lenstra TL, van Leenen D, Groot Koerkamp MJ, Margaritis T, Brok MO,
773 Kemmeren P, Holstege FC. Cell cycle population effects in perturbation studies. Mol Syst Biol. 2014 Jun;
774 10:732. doi: 10.15252/msb.20145172.

775 **Orlando DA**, Lin CY, Bernard A, Wang JY, Socolar JE, Iversen ES, Hartemink AJ, Haase SB. Global control of
776 cell-cycle transcription by coupled CDK and network oscillators. Nature. 2008 Jun; 453(7197):944–947. doi:
777 10.1038/nature06955.

778 **Parkhomchuk D**, Borodina T, Amstislavskiy V, Banaru M, Hallen L, Krobitsch S, Lehrach H, Soldatov A. Tran-
779 scriptome analysis by strand-specific sequencing of complementary DNA. Nucleic Acids Res. 2009 Oct;
780 37(18):e123. doi: 10.1093/nar/gkp596.

781 **Paulo JA**, O'Connell JD, Everley RA, O'Brien J, Gygi MA, Gygi SP. Quantitative mass spectrometry-based mul-
782 tiplexing compares the abundance of 5000 *S. cerevisiae* proteins across 10 carbon sources. Journal of
783 Proteomics. 2016; 148:85–93. https://www.sciencedirect.com/science/article/pii/S1874391916303013, doi:
784 https://doi.org/10.1016/j.jprot.2016.07.005.

785 **Porro D**, Martegani E, Ranzi BM, Alberghina L. Oscillations in continuous cultures of budding yeast: a segregated
786 parameter analysis. Biotechnol Bioeng. 1988 Aug; 32(4):411–417. doi: 10.1002/bit.260320402.

787 **Pronk JT**, Yde Steensma H, Van Dijken JP. Pyruvate metabolism in *Saccharomyces cerevisiae*. Yeast. 1996 Dec;
788 12(16):1607–1633. doi: 10.1002/(SICI)1097-0061(199612)12:16<1607::AID-YEA70>3.0.CO;2-4.

789 **Pu S**, Wong J, Turner B, Cho E, Wodak SJ. Up-to-date catalogues of yeast protein complexes. Nucleic Acids Res.
790 2009 Feb; 37(3):825–831. doi: 10.1093/nar/gkn1005.

791 **Sasidharan K**, Amariei C, Tomita M, Murray DB. Rapid DNA, RNA and protein extraction protocols optimized
792 for slow continuously growing yeast cultures. Yeast. 2012 Aug; 29(8):311–322. doi: 10.1002/yea.2911.

793 **Satroutdinov AD**, Kuriyama H, Kobayashi H. Oscillatory metabolism of *Saccharomyces cerevisiae* in continuous
794 culture. FEMS Microbiol Lett. 1992 Nov; 77(1-3):261–267. doi: 10.1016/0378-1097(92)90167-m.

795 **Schaechter M**, Maaløe O, Kjeldgaard NO. Dependency on medium and temperature of cell size and chemical
796 composition during balanced growth of *Salmonella typhimurium*. J Gen Microbiol. 1958 Dec; 19(3):592–606.

797 **Scott M**, Gunderson CW, Mateescu EM, Zhang Z, Hwa T. Interdependence of cell growth and gene expression:
798 origins and consequences. Science. 2010 Nov; 330(6007):1099–1102. doi: 10.1126/science.1192588.

799 **Silverman SJ**, Petti AA, Slavov N, Parsons L, Briehof R, Thiberge SY, Zenklusen D, Gandhi SJ, Larson DR,
800 Singer RH, Botstein D. Metabolic cycling in single yeast cells from unsynchronized steady-state popula-
801 tions limited on glucose or phosphate. Proc Natl Acad Sci U S A. 2010 Apr; 107(15):6946–6951. doi:
802 10.1073/pnas.1002422107.

803 **Slavov N**, Botstein D. Coupling among growth rate response, metabolic cycle, and cell division cycle in yeast.
804 Mol Biol Cell. 2011 Jun; 22(12):1997–2009. doi: 10.1091/mbc.E11-02-0132.

805 **Slavov N**, Macinskas J, Caudy A, Botstein D. Metabolic cycling without cell division cycling in respiring yeast.
806 Proc Natl Acad Sci U S A. 2011 Nov; 108(47):19090–19095. doi: 10.1073/pnas.1116998108.

807 **Sonnleitner B**, Käppeli O. Growth of *Saccharomyces cerevisiae* is controlled by its limited respiratory ca-
808 pacity: Formulation and verification of a hypothesis. Biotechnol Bioeng. 1986 Jun; 28(6):927–937. doi:
809 10.1002/bit.260280620.

810 **Strässle C**, Sonnleitner B, Fiechter A. A predictive model for the spontaneous synchronization of *Saccharomyces*
811 *cerevisiae* grown in continuous culture. II. Experimental verification. Journal of Biotechnology. 1989; 9(3):191 –
812 208. http://www.sciencedirect.com/science/article/pii/0168165689901089, doi: 10.1016/0168-1656(89)90108-9.

813 **Thaben PF**, Westermark PO. Detecting rhythms in time series with RAIN. J Biol Rhythms. 2014 Dec; 29(6):391–
814 400. doi: 10.1177/0748730414553029.

815 **Tu BP**, Kudlicki A, Rowicka M, McKnight SL. Logic of the yeast metabolic cycle: temporal compartmentalization
816 of cellular processes. Science. 2005 Nov 18; 310(5751):1152–8.

817 **Verduyn C**, Stouthamer AH, Scheffers WA, van Dijken JP. A theoretical evaluation of growth yields of yeasts.
818 Antonie Van Leeuwenhoek. 1991 Jan; 59(1):49–63.

819 **Waldron C**, Lacroute F. Effect of growth rate on the amounts of ribosomal and transfer ribonucleic acids in
820 yeast. J Bacteriol. 1975 Jun; 122(3):855–865.

821 **Wang GZ**, Hickey SL, Shi L, Huang HC, Nakashe P, Koike N, Tu BP, Takahashi JS, Konopka G. Cycling Transcrip-
822 tional Networks Optimize Energy Utilization on a Genome Scale. Cell Rep. 2015 Dec; 13(9):1868–1880. doi:
823 10.1016/j.celrep.2015.10.043.

824 **Wang Y**, Song L, Liu M, Ge R, Zhou Q, Liu W, Li R, Qie J, Zhen B, Wang Y, He F, Qin J, Ding C. A proteomics
825 landscape of circadian clock in mouse liver. Nature Communications. 2018 Apr; 9(1):1553.

826 **Xia J**, Sanchez BJ, Chen Y, Campbell K, Kasvandik S, Nielsen J. Proteome allocations change linearly with the spe-
827 cific growth rate of *Saccharomyces cerevisiae* under glucose limitation. Nat Commun. 2022 May; 13(1):2819.
828 doi: 10.1038/s41467-022-30513-2.

829 **Xu Z**, Yaguchi S, Tsurugi K. Gts1p stabilizes oscillations in energy metabolism by activating the transcription of
830 TPS1 encoding trehalose-6-phosphate synthase 1 in the yeast *Saccharomyces cerevisiae*. Biochem J. 2004 Oct;
831 383(Pt 1):171–178. doi: 10.1042/BJ20040967.